Draft version September 20, 2016
Preprint typeset using LaTeX style emulateapj v. 01/23/15

THE PALE GREEN DOT: A METHOD TO CHARACTERIZE PROXIMA CENTAURI b USING EXO-AURORAE

Rodrigo Luger[1,3,4,6], Jacob Lustig-Yaeger[1,3,4], David P. Fleming[1,3,5], Matt A. Tilley[2,3,4], Eric Agol[1,3,4], Victoria S. Meadows[1,3,4], Russell Deitrick[1,3,4], and Rory Barnes[1,3,4]

Draft version September 20, 2016

ABSTRACT

We examine the feasibility of detecting auroral emission from the potentially habitable exoplanet Proxima Centauri b. This planet's active, late-type M dwarf host makes detection of aurorae more favorable, primarily by increasing auroral power and improving the planet-star contrast in the visible wavelength range due to strong TiO absorption in the star. Detection of aurorae would yield an independent confirmation of the planet's existence, constrain the presence and composition of its atmosphere, and determine the planet's eccentricity and inclination, thereby breaking the mass-inclination degeneracy. We use two independent methods to estimate that the auroral power on Proxima b is $\sim$100$\times$ stronger than that on Earth under steady-state stellar wind if Proxima b is a terrestrial world with an atmosphere and magnetic field. These estimates indicate a planet-star contrast ratio of $\gtrsim 10^{-6}$ in a narrow band about the green 5577Å OI auroral emission line, although higher contrast may be possible during periods of magnetospheric disturbance. We find that detection of 10 terawatt aurorae may be possible with 10 meter class facilities in $\sim$1 day of exposure time with a signal-to-noise ratio of 6 if used in combination with visible-light adaptive optics and coronagraphic starlight suppression. We searched the high spectral resolution Proxima b HARPS data for the 5577Å line and for other prominent oxygen and nitrogen lines, but find no signal, indicating that oxygen green line auroral emission on Proxima Centauri must be below $\sim 10^{15}$ W ($\sim 3 \times 10^4$ times stronger than on Earth), consistent with our predictions. Future detection with a large-aperture, space-based coronagraphic telescope or a ground-based extremely large telescope with coronagraph could push sensitivity down to terawatt oxygen aurorae with exposure times of $\sim$100 hours at high spectral resolution.

Subject headings: planets and satellites: terrestrial planets, atmospheres, aurorae, detection — Proxima Centauri b

1. INTRODUCTION

The discovery of Proxima Centauri b (henceforth 'Proxima b'), at only 1.3pc from the Sun, ushers in a new era of potentially habitable exoplanet science because of the rich characterization potential afforded by its proximity (Anglada-Escudé et al. 2016). Although Proxima b is not known to transit—making transmission spectroscopy impossible—it is an ideal candidate for high-contrast direct spectroscopy using an extremely large coronagraph-equipped telescope. However, even with the enhancement in angular resolution provided by the proximity of its host star, Proxima b's close-in orbit (a = 0.0485 AU; Anglada-Escudé et al. 2016) precludes imaging with current coronagraphs, such as the Gemini Planet Imager (GPI; Macintosh et al. 2014) and the Very Large Telescope's Spectro-Polarimetric High-contrast Exoplanet REsearch (VLT-SPHERE; Beuzit et al. 2008), which operate primarily in the near-infrared. This is in part due to the poorer Strehl ratios currently achievable at visible wavelengths with ground-based adaptive optics (AO) systems[7]. Consequently, in advance of larger diameter ground- and space-based telescopes, and improvements in visible AO systems, we must initially consider observations that do not rely on transits or current coronagraphy to search for and characterize the atmosphere of Proxima b.

Phase curves may offer one of the first means to study the atmosphere of Proxima b (Turbet et al. 2016; Kreidberg & Loeb 2016; Meadows et al. 2016) by potentially showing the reduction in day-night thermal emission contrast associated with an atmosphere. Phase curves have proven to be a successful means to characterize the atmospheres of planets larger and hotter than Proxima b (Cowan et al. 2007; Knutson et al. 2007; Knutson et al. 2008; Crossfield et al. 2010; Brogi et al. 2012; Zellem et al. 2014; Stevenson et al. 2014), including ones that do not transit (Selsis et al. 2011; Faigler & Mazeh 2011; Maurin et al. 2012; Brogi et al. 2014). However, the expected planet-to-star contrast ratio in the visible and NIR due to reflected stellar radiation is likely to be below the anticipated systematic noise floor for JWST/NIRSpec (Meadows et al. 2016), and although the planet-star contrast ratio becomes quite favorable beyond 10 μm, where the planetary thermal emission peaks, mid-IR phase curves will require JWST/MIRI. Given the uncertainty of the expected phase-curve studies with JWST, it is worthwhile to investigate novel methods for characterizing the atmospheric state of Proxima b.

To complement the anticipated JWST thermal phase

[1] Astronomy Department, University of Washington, Box 951580, Seattle, WA 98195
[2] Department of Earth & Space Sciences, University of Washington, Box 351310, Seattle, WA 98195
[3] NASA Astrobiology Institute – Virtual Planetary Laboratory Lead Team, USA
[4] Astrobiology Program, University of Washington, 3910 15th Ave. NE, Box 351580, Seattle, WA 98195, USA
[5] eScience Institute, University of Washington, Seattle, WA, USA
[6] rodluger@uw.edu

[7] See, e.g., https://www.eso.org/sci/facilities/paranal/instruments/sphere/ove

curve measurements, in this work we explore the possibility of directly detecting optical auroral emission from the atmosphere of Proxima b using high-resolution optical spectroscopy. Numerous studies have investigated exoplanet aurorae in the radio due to cyclotron and synchrotron emission to constrain the planetary magnetic field (e.g. Bastian et al. 2000; Grießmeier et al. 2007; Zarka 2007; Hess & Zarka 2011; Driscoll & Olson 2011). Smith et al. (2004) modeled the role of aurorae in redistributing high energy incident stellar flux to the surface of terrestrial exoplanets, and the effect of aurorae on the optical and infrared spectra of gaseous exoplanets has been considered (Rimmer et al. 2015). However, the detection of auroral emission from the atmosphere of nearby terrestrial exoplanets and the physical constraints imposed by such a detection have not been fully discussed.

Detecting optical auroral emission from the possible atmosphere of Proxima b is likely much more favorable for this system than for an Earth-Sun analog. This is due to both planetary and stellar characteristics that favor auroral production and improve detectability. In particular, Proxima b's intrinsic planetary properties may favor production of aurorae from O atoms. If Proxima b is Earth-like in composition, recent dynamical/planetary interior modeling results by Barnes et al. (2016) and Zuluaga & Bustamante (2016) suggest that the planet is likely to have a magnetic field, potentially increasing the likelihood of atmospheric retention and of auroral emission. Atmospheres rich in oxygen-bearing molecules, including O_2 and CO_2, have been predicted for Proxima b (Meadows et al. 2016) as a result of the evolutionary processes for terrestrial planets orbiting M dwarfs (Luger & Barnes 2015; Barnes et al. 2016). On Earth, the oxygen auroral line at 5577Å provides the distinctive green glow observed in both the Aurora Borealis[8] and the Aurora Australis, and is the brightest auroral feature (Chamberlain 1961; Dempsey et al. 2005). For emissions from the upper atmosphere, only the 1.27μm O_2 airglow and combined near-infrared OH nightglow features are brighter (Hunten et al. 1967). The oxygen green line is seen in both the Earth's O_2-rich atmosphere (Chamberlain 1961) and Venus' CO_2-dominated atmosphere (Slanger et al. 2001), where it has been observed to increase in brightness after CME events (Gray et al. 2014).

The stellar properties and the planet-star separation are also likely to enhance the auroral power on Proxima b relative to an Earth-Sun analog. Proxima Centauri is an active flare star with a magnetic field $\sim$600$\times$ stronger than that of the Sun (Reiners & Basri 2008; Davenport et al. 2016). Since stellar activity drives auroral emission, such features may be much stronger on planets orbiting active M dwarfs. Additionally, with a close-in orbit of 0.0485 AU, Proxima b is about 20$\times$ closer to Proxima Centauri than the Earth is to the Sun (Anglada-Escudé et al. 2016). This proximity further increases particle fluxes incident on the planetary atmosphere that drive ionization and the subsequent recombination radiation.

In addition to increasing the likelihood and strength of the aurora, the characteristics of the Proxima Centauri system may also enhance its detectability. Since the Proxima system is only 1.3pc away, it is perhaps the best-case scenario for the detection of the faint auroral signal from a terrestrial exoplanet. Even though the planet-star contrast ratio in reflected visible light is poor ($\sim 10^{-7}$; see Turbet et al. 2016; Kreidberg & Loeb 2016; Meadows et al. 2016), if Proxima b exhibits auroral emission, this will brighten the planet and boost the planet-star contrast by a few orders of magnitude at the wavelengths of the auroral emission features. The short wavelength of the oxygen green line also improves the contrast of the planet relative to the star due to the star's cool temperature and TiO absorption, which strongly suppresses the brightness of the star in the visible. This improvement in contrast is significantly less for the near-infrared O_2 1.27μm and OH airglow lines. In addition to increasing the contrast, the small semi-major axis of Proxima b results in an orbital velocity of $\sim$50 km/s, which will cause its auroral emission to be Doppler-shifted by as much as 1Å over the course of its orbit, making it easier to disentangle it from stellar features via high resolution spectroscopy. An additional advantage of the short wavelength is the smaller inner working angle and point-spread function that may be achieved with a coronagraph at shorter wavelength (Agol 2007). These factors all improve the chance of detection with ground-based telescopes.

The detection of the oxygen auroral line at 5577Å would provide an important diagnostic for planetary properties. Its detection would not only confirm the presence of the planet, but would point to the presence of an atmosphere with abundant oxygen atoms, which is more likely to indicate a terrestrial body. Additionally, the detection of the line would yield a measurement of the radial velocity (RV) of the planet, which combined with the RV measurements of the star (Anglada-Escudé et al. 2016) would enable the measurement of the eccentricity and inclination of the orbit, ultimately yielding the mass of the planet. Detection of the oxygen auroral line would therefore provide several key planetary parameters that could be used to constrain Proxima b's potential habitability (Barnes et al. 2016; Meadows et al. 2016).

This paper is organized as follows: in §2 we calculate the expected total auroral emission strength of Proxima b. In §3 we model the planet-star contrast ratio assuming oxygen auroral emission and calculate the integration time required to detect the feature. In §4 we conduct a preliminary search for auroral emission in the HARPS high-resolution, ground-based spectroscopy used by Anglada-Escudé et al. (2016) for the RV detection of Proxima b. Finally, in §5 we discuss our results and present our conclusions.

2. AURORAL SIGNAL STRENGTH

Below, we quantitatively estimate the auroral intensity for steady-state stellar input. We employ two different methods to compare and contrast the regimes for both an Earth-like and a Neptune-like planetary magnetic dipole moment and anticipated auroral production efficiency. Both planets are assumed to be terrestrial bodies with the orbital characteristics of Proxima b. Method 1 involves a simple estimation of the auroral brightness driven by the stellar wind power delivered at the magnetopause of the planet. Method 2 uses the prediction of a magnetohydrodynamical (MHD) model that

[8] Also known as the Northern Lights, which enables nighttime-viewing of queer sights (Service 1907).

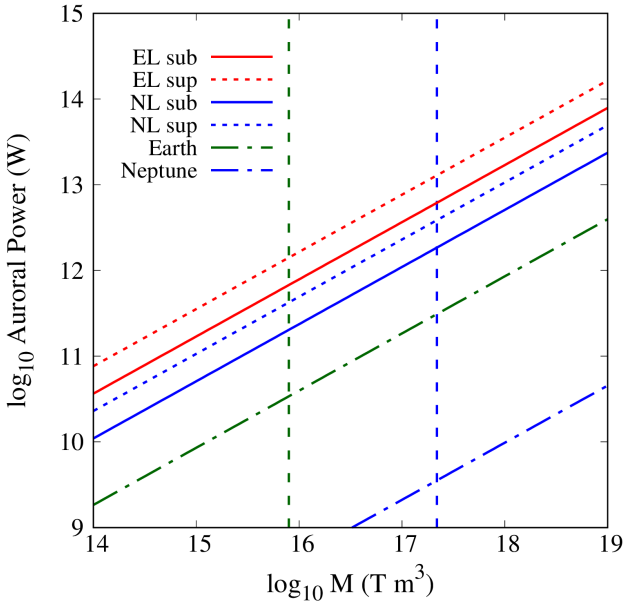

FIG. 1.— Estimated auroral power as a function of planetary magnetic dipole moment calculated using the stellar wind scaling method from §2.1. Solid (dotted) lines correspond to the sub-(super-)Alfvénic stellar wind conditions. Red (blue) lines correspond to an Earth-like (Neptune-like) planetary magnetic dipole with conversion efficiency of ∼1% (∼0.3%). The green (blue) dash-dotted lines correspond to Earth (Neptune) in its natural orbit around the Sun. The dashed vertical green (blue) line indicates the magnitude of Earth's (Neptune's) magnetic dipole moment.

was empirically tuned to calculate the auroral response at Earth, with modifications to the relevant inputs of the stellar wind of Proxima Centauri and assumed planetary parameters for Proxima b (Anglada-Escudé et al. 2016).

The quantities we calculate include only the localized emissions caused by magnetospheric particle precipitation into a discrete auroral oval, not the diffuse, global phenomenon of airglow. On Earth, the 5577Å airglow can be visible to the naked eye and could be significant on Proxima b, but is driven by different physical processes (e.g., nighttime recombination due to dayside photoionization) that are out of scope for this analysis. Similarly, the 5577Å airglow has been observed at Venus (e.g. Slanger et al. 2001) and Mars (e.g. Seth et al. 2002) — both of which have no global magnetic field. For these reasons we cannot suggest basing the existence of or placing constraints on Proxima b's planetary magnetic field based on the detection of this auroral line.

2.1. *Auroral stellar wind power scaling*

M dwarf mass-loss rates, and therefore stellar winds, are not well constrained due to observational sparsity and difficulty (e.g. Wood et al. 2004). To model the M dwarf winds for Proxima Centauri, we adopt the predictions from the modeling efforts of Cohen et al. (2014), who generated an MHD stellar wind model for the M3.5 star EV Lacertae based on available observations. Wood et al. (2005) estimated that the mass-loss per unit surface area for Proxima Centauri and EV Lacertae as quite similar, which sets the wind conditions at distances in stellar radii to be comparable. Here, we consider both super- and sub-Alfvénic conditions for the steady-state stellar wind, using the reported parameters at Planet C (simulated for $a \approx 90R_\star$, similar to Proxima b) from Cohen et al. (2014); see Table 1.

TABLE 1
STELLAR WIND CONDITIONS

Quantity	Sub-Alfvénic	Super-Alfvénic
n (cm^{-3})	46	123
T (10^5 K)	4.98	1.9
u (km s^{-1})	(-728, -50, -17)	(-660, 8, 14)
B (nT)	(240, 88, 17)	(-244, 74, 18)
M_A	0.88	1.3

NOTE. — Stellar wind conditions from Cohen et al. (2014).

The stellar wind power delivered to the magnetosphere of the planet can be expressed as

$$P_{SW} = \rho v^3 \pi R_{MP}^2, \quad (1)$$

where ρ and v are the stellar wind mass density and velocity, respectively, and R_{MP} is the magnetopause distance along the line connecting the star and planet (sub-stellar point). The latter can be estimated through magnetospheric pressure balance with the total stellar wind pressure:

$$\frac{\mathcal{M}^2}{2\mu_0 R_{MP}^6} = p_{KE} + p_{ram} + p_B, \quad (2)$$

where $\mathcal{M}$ represents the magnitude of the magnetic dipole moment and R_{MP} is the distance from the planet at which the magnetic pressure of the planet balances the pressure of the stellar wind. The terms on the RHS of Eq. 2 represent the kinetic ($p_{KE} = nk_BT$), dynamic ram ($p_{ram} = \rho v^2$), and magnetic ($p_B = B_{SW}/2\mu_0$) pressures of the stellar wind, calculated from the values in Table 1. For the Earth-like, EL, (Neptune-like, NL) magnetosphere, we assume a magnetic dipole moment of $\mathcal{M} = 8.0{\times}10^{15}$ ($2.2{\times}10^{17}$) Tesla m^3. Solving for R_{MP} in Eq. 2 and inserting into Eq. 1 provides an estimate of the stellar wind power incident on the planetary magnetopause. Externally-driven planetary auroral systems are not typically 100% efficient at converting the incident stellar wind power into auroral emission, and range from ∼0.3% at Neptune, ∼1% at Earth, and up to ∼100% at Jupiter (e.g. Cheng 1990; Bhardwaj & Gladstone 2000). For reference, at Earth, this method gives us a reasonable estimate of the total auroral power of ∼30 GW for nominal solar wind conditions (5 cm^{-3}, 400 km s^{-1}, 10 eV protons), which is consistent with the anticipated power of 1-100 GW, depending on solar and magnetospheric activity.

Fig. 1 shows the predicted auroral power from Eq. 1 for both EL and NL planetary magnetic dipole moments and conversion efficiencies in both the sub- and super-Alfvénic stellar wind conditions from Table 1. Auroral power estimates for both the EL and NL planets at 0.05 AU are shown in Table 2. The total emitted power ranges from ∼22.3× Earth's auroral emission (EL, sub-Alfvénic) to ∼130× (NL, super-Alfvénic). Note that discussion of a true, ∼17.15 Neptune-mass planet is included below in § 2.2.

TABLE 2
Calculated emitted total auroral power, by method

Case	Method 1 [TW]	Method 2 [TW]
EL_{Sub}	0.68	1.09
NL_{Sub}	1.86	10.00
EL_{Sup}	1.42	1.09
NL_{Sup}	3.88	10.00

Note. — Total emitted power for the Earth-like (EL) and Neptune-like (NL) planets in the sub-Alfvénic (Sub) and super-Alfvénic (Sup) stellar wind.

Note that Neptune's magnetic field is highly inclined, rotationally offset, and relatively complex with significant quadrupole/octupole moments that have similar or higher magnitude than the dipole moment; in the present work, we have assumed a simple, untilted dipole field, with equatorial strength equal to that reported by Voyager 1 observations (e.g. Connerney et al. 1991; Mauk & Bagenal 2012). The auroral power estimate for Neptune in Fig. 1 (∼3 GW) makes these same geometric assumptions, leading to an overestimate when compared to the actual auroral power emitted at Neptune.

We scale the total auroral power values in Table 2 by 60% (assuming lower energy particle populations present in a quiescent magnetosphere) to obtain estimated emission power of the OI 5577Å line (Chamberlain 1961; Kivelson & Russell 1995). From this method, we predict an emitted power of ∼0.41 (1.12) TW for the EL (NL) planet in the sub-Alfvénic stellar wind, and ∼0.852 (2.33) TW for the super-Alfvénic conditions for the 5577Å line.

2.2. *3D MHD empirical energy coupling*

Wang et al. (2014) developed a global, 3D MHD model to obtain a nonlinear fit to the energy coupling function to estimate the energy transferred from the solar wind to Earth's auroral activity (see their Eq. 13). As this system takes into account only the Earth's magnetosphere, we require it to scale to other planetary magnetic fields – such as Neptune's – by noting the coupling scales with the planetary magnetic dipole magnitude, $\mathcal{M}_P^{2/3}$ (Vasyliunas et al. 1982). Therefore, $(\mathcal{M}_{Nep}/\mathcal{M}_{Earth})^{2/3} \approx 9.1$, which we can fold into the coupling constant for an NL planet.

Wang et al. (2014) estimate the fraction of total solar wind energy input to the entire magnetosphere is ∼13% of the incident energy. They further estimate that 12% of that energy is dissipated by particle precipitation in the auroral regions, yielding a total solar wind/auroral coupling efficiency of ∼1.56% – very similar to the value assumed in § 2.1 for the EL planet. This method predicts a maximum coupling of auroral particle precipitation (with interplanetary magnetic field clock angle $\theta = \pi$, driving reconnection and likely substorm activity) at Earth (Neptune) of ∼222.6 (2.8) GW, which is in order of magnitude agreement with terrestrial plasma observations (e.g. Hubert et al. 2002) and inferred values from Voyager UV measurements (e.g. Sandel et al. 1990; Mauk et al. 1994).

For Proxima b, this method predicts a total power of auroral particle precipitation of 11.82 (107.55) TW for the EL (NL) planet in the sub-Alfvénic stellar wind, and 12.39 (112.78) TW in the super-Alfvénic wind. To compare directly to the total auroral power output such as that calculated in § 2.1, we must link these values to the aurora by including the efficiency of precipitating charged particles in the production of auroral emission for the 5577Å line, as below.

Steele & McEwen (1990) reported coordinated ground-based observations of auroral line intensities and the related satellite observations of energetic electron flux to draw a relation between electron precipitation and auroral brightness. For the 5577Å OI line, 1.73±0.51 (1.23±0.44) kR/(erg cm^{-2} s^{-1}) was observed for a Maxwellian electron population of characteristic temperature 1.8 (3.1) keV, which corresponds to an efficiency of 0.62% (0.44%) in conversion of incident flux to OI flux (1 R $\equiv 10^6/4\pi$ s^{-1} cm^{-2} sr^{-1}). It is worth noting that the fraction of total hemispheric particle energy delivered by electrons is ∼80%, varying by 10-20% due to magnetospheric activity (Hubert et al. 2002).

The magnetopause distance we calculated via Eq. 2 for the EL (NL) magnetic dipole moment, ∼5.7 (17.2) R_P, can provide a simple estimate of the total auroral oval coverage. The magnetic co-latitude of the boundary between open and closed flux is $\sin^{-1}(1/\sqrt{R_{MP}})$; if we assume a nominal 5° auroral oval width centered at the co-latitude obtained, we calculate a single-hemisphere coverage of ∼9.2×10^{16} (5.2×10^{16}) cm^2 for the auroral oval of the EL (NL) planet.

Using the average of the efficiencies given by Steele & McEwen (1990) above, we obtain a brightness value of 1.59 (25.8) MR for the EL (NL) planet for the 5577Å line for the sub- and super-Alfvénic conditions. This corresponds to an emission power of ∼0.65 (6) TW for the 5577Å line per hemisphere. Assuming that 60% of auroral power is emitted as the 5577Å line under nominal, non-substorm conditions, we obtain a total auroral power of 1.1 (10) TW. These values are comparable to those obtained in § 2.1, and more favorable for the stronger NL dipole, as expected. Note that the values are similar for the sub- and super-Alfvénic cases, as the method from Wang et al. (2014) is weighted more heavily towards the velocity and IMF clock angle of the stellar wind; as seen in Table 1, the wind parameters are comparable in most regards, including the velocity and clock angle, and therefore give matching results within 5%.

If Proxima b is, instead, a planet of Neptune mass and radius (as opposed to our assumption of only the magnetic parameters) on a close to face-on orbit, it will have an upper atmosphere dominated by H/H_2. Therefore the above calculations are not applicable, and we should consider FUV emission in lieu of OI or N_2^+ lines. Voyager UV observations reported by Sandel et al. (1990) estimated the localized FUV (967-1115 Å) auroral brightness as ∼5 R. Mauk et al. (1994) found that the electron flux to drive the observed UV aurora at Neptune was ∼10^{-3} erg cm^{-2} s^{-2}. Therefore we infer a conversion efficiency for Neptune's aurora in the 967-1115 Å bandpass to be ∼5 kR/(erg cm^{-2} s^{-1}), corresponding to ∼9.9%. This gives us a scaled FUV brightness of ∼4.02 (4.22) MR for the sub-(super-)Alfvénic stellar wind conditions for the Neptune-like planet, or 19.43 (20.39) TW over the 967-1115 Å band. While this is significantly stronger than the

OI emission of an Earth-like planet, it may be harder to detect given both the width of this band and the fact that if Proxima b is Neptune-like, its orbital inclination must be $\lesssim 5°$, making deconvolution from stellar lines more difficult (see §4).

It is possible that all the auroral numbers reported for the sub-Alfvénic cases above could be a factor of 4-5 (or more) larger. We are assuming a simple dipolar, Earth-Sun like interaction with the sub-Alfvenic stellar wind, which isn't specifically the case for sub-Alfvenic flow; these interactions are more akin to the interactions of Ganymede and Io with the corotating magnetosphere of Jupiter, with the formation of Alfven wings. Modeling efforts by Preusse et al. (2007) showed that for a giant planet with a dipole magnetic moment, field-aligned currents (which are associated with auroral activity) are significantly stronger for planets orbiting inside the Alfvén radius of their stellar host. Our estimates, therefore, could be viewed as lower limits. It is also worth noting that Cohen et al. (2014) suggested that a transition between the sub- and super-Alfvénic conditions would likely produce enhanced magnetospheric activity and therefore could lead to a periodicity in the auroral activity depending on combined planetary orbital and stellar rotational phases. For Earth, the diffuse airglow at 5577 Å can be significant ($\geq$ 1 kR), but the anticipated magnitude at Proxima b is unknown, and could be another factor that contributes to the overall signal. Detailed photochemical modeling is required to obtain an estimate of airglow production.

In summary, we predict an auroral emission at 5577Å that is of order 10-100 times stronger than seen on Earth for steady-state stellar wind conditions and a quiet magnetosphere, corresponding to a total auroral power on the order of $\sim$1 TW for an Earth-like terrestrial planet orbiting Proxima Centauri. The predicted values will naturally change based on planetary parameters (e.g., magnetic dipole moment, magnetospheric particle energy distributions, substorm onset, atmospheric Joule heating) and stellar activity. By our analysis, the $\sim 10^3$ enhancement compared to Earth as suggested by O'Malley-James & Kaltenegger (2016) is possible only during transient magnetospheric conditions, if Proxima b's magnetic dipole is significantly stronger than Earth's, or if stellar mass-loss is higher than predicted (Wood et al. 2005; Cohen et al. 2014).

3. AURORAL DETECTABILITY

Using the auroral power estimates from §2, we explore the feasibility of detecting the 5577Å OI auroral emission line with five different ground-based telescope configurations: the 3.6m High Accuracy Radial velocity Planet Searcher (HARPS), the 8.2m Very Large Telescope (VLT) with and without a coronagraph, and a Thirty Meter Telescope (TMT) concept with and without a coronagraph. We also model the detection using two future space-based coronagraph concepts: the 16m Large UV/Optical/IR Surveyor (LUVOIR; Kouveliotou et al. 2014; Dalcanton et al. 2015) and the 6.5m Habitable Exoplanet Imaging Mission (HabEX; Mennesson et al. 2016). Although the expected resolving power for future space-based coronagraph missions is expected to be $R\sim$100 to resolve molecular bands in the optical and NIR (Robinson et al. 2016), high-resolving power ($R \gtrsim 30,000$) would be required to detect the OI line. The OI 5577Å green line has no hyperfine structure and negligible natural width (Hunten et al. 1967), making it best suited to detection using high resolution spectroscopy. Broader spectral resolution element widths allow more stellar continuum to contaminate the sharp planetary emission signal and decrease the planet-star contrast. High spectral resolution coronagraphy with the VLT will require an update to the SPHERE high-contrast imager and a coupling with the ESPRESSO spectrograph, as described in Lovis et al. (2016). Our HARPS and TMT telescope models assume $R \equiv \lambda/\Delta\lambda = 115,000$, while for VLT we use $R = 120,000$. All models assume a total throughput of 5% and a quantum efficiency of 90%. Coronagraph noise estimates use the model presented in Robinson et al. (2016) with updated parameters from Meadows et al. (2016), and consider noise due to speckles, dark counts, read noise, telescope thermal emission, and zodi and exozodi light. Ground-based coronagraphy assumes a conservative design contrast of 10^{-5} (Dou et al. 2010; Guyon et al. 2012), while space-based assumes 10^{-10} following Meadows et al. (2016). Non-coronagraph telescope calculations assume only stellar noise at the photon limit; their values are therefore lower limits.

Our integration time calculations follow those described in Robinson et al. (2016). For the stellar spectrum we adopt the steady-state Proxima Centauri spectrum of Meadows et al. (2016) and neglect the impact of flares on the stellar continuum. We assume that the quoted total auroral power is constant throughout the entire observation with 60% of the energy emitted via the 5577Å OI line (Chamberlain 1961; Kivelson & Russell 1995).

For observations without a coronagraph, both the stellar flux and reflected stellar flux define the continuum from which we wish to resolve the auroral emission feature. Observations with a coronagraph need only resolve the auroral emission above the coronagraph noise and reflected stellar continuum. With these considerations in mind, we simulate the net planetary emission as a combination of reflected stellar continuum and auroral emission. We compute the flux from the reflected stellar continuum by assuming that the planet is a Lambertian scatterer at quadrature with a planetary geometric albedo of 0.3 and a planetary radius of 1.07 $R_\oplus$ following Barnes et al. (2016). We then inject the expected flux from the given auroral line at its central wavelength. We integrate over all spectral elements that contain the auroral line flux, taking the auroral photon count rate as our signal and all other sources as noise as in Robinson et al. (2016). For the oxygen 5577Å line and our nominal resolving power, this corresponds to $\sim$0.1Å, or about two spectral elements.

Table 3 shows the integration times required to achieve a signal-to-noise of 6 on the 5577Å OI auroral emission line above the stellar and reflected planetary continuum as a function of total auroral power. We simulated contrast ratios and integration times for total emitted auroral powers ranging from $10^9 - 10^{15}$ W to bracket all potential auroral fluxes. The 10^9 W lower limit represents an aurora roughly 10$\times$ weaker than Earth's, while the upper limit of 10^{15} W is an extreme case that is $10^3\times$

TABLE 3
Planet-Star contrast ratios and integration times necessary to detect the 5577Å OI emission line at a signal-to-noise of 6 as a function of total auroral power.

		Integration Time [hours]						
Total Auroral Power [W]	Planet-Star Contrast	HARPS	VLT	VLT + C	TMT	TMT + C	HabEX	LUVOIR
10^{9}	9×10^{-8}	1×10^{14}	2×10^{13}	1×10^{9}	2×10^{12}	5×10^{7}	2×10^{9}	5×10^{7}
10^{10}	1×10^{-7}	1×10^{12}	2×10^{11}	1×10^{7}	2×10^{10}	5×10^{5}	2×10^{7}	5×10^{5}
10^{11}	3×10^{-7}	1×10^{10}	2×10^{9}	1×10^{5}	2×10^{8}	5×10^{3}	2×10^{5}	5×10^{3}
10^{12}	2×10^{-6}	1×10^{8}	2×10^{7}	1×10^{3}	2×10^{6}	60	2×10^{3}	60
10^{13}	2×10^{-5}	1×10^{6}	2×10^{5}	20	2×10^{4}	9×10^{-1}	30	2
10^{14}	2×10^{-4}	1×10^{4}	2×10^{3}	7×10^{-1}	2×10^{2}	5×10^{-2}	1	2×10^{-1}
10^{15}	2×10^{-3}	1×10^{2}	20	6×10^{-2}	2	4×10^{-3}	9×10^{-2}	2×10^{-2}

Note. — We assume that 60% of the total aurora power is emitted in the OI line. Integration times assume a telescope throughput of 5%, a spectrograph with resolution $\lambda/\Delta\lambda = 115,000$ for the HARPS and TMT analogs and $\lambda/\Delta\lambda = 120,000$ for the VLT analog. "+ C" indicates the use of a coronagraph and associated noise sources discussed in Robinson et al. (2016). Total auroral powers in the range $10^{12} - 10^{13}$ W roughly correspond to those predicted in §2.

stronger than our estimated Proxima b value of 10^{12} W. Although unlikely, an aurora of 10^{15} W could be possible for rare, transient events such as during a large flare from Proxima Centauri.

The weak 10^{9} W aurora is indistinguishable from the purely reflecting planet-star contrast near the 5577Å OI auroral emission line (Turbet et al. 2016; Kreidberg & Loeb 2016; Meadows et al. 2016) and effectively demonstrates why high resolution spectroscopy is not typically considered for high-contrast coronagraphy. However, the presence of a strong emission line that boosts the contrast in a narrow $\Delta\lambda$ can justify the use of high-resolution spectroscopy. For an Earth-like planet, the total auroral power estimates from §2 ($\sim 10^{12}$ W) make detecting the OI emission line impractical with current instruments, even though the contrast ratio at the line is relatively strong ($\sim 10^{-6}$). For instance, between $10^{7} - 10^{8}$ hours of photon-limited exposure time would be required to detect OI emission with HARPS or VLT, assuming the photon-noise limit could be achieved. However, vigorous stellar activity (Davenport et al. 2016) is likely to contribute greatly to the noise, such that actual integration times would be much higher. Though unlikely, if the auroral power were much higher ($\sim 10^{15}$ W), detection of OI emission should be possible with current instruments in only a few tens of hours to one hundred hours of integration time, assuming rigorous data reduction and analysis (e.g. Brogi et al. 2012). The detection of aurorae with power $\sim 10^{12}$ W will likely require the development of robust AO systems that operate in the visible and high spectral resolution coronagraphy to focus on the narrow line and suppress the stellar emission.

For a SPHERE-ESPRESSO coupling (Lovis et al. 2016), the integration times required to detect an OI auroral line are more favorable over a wide range of possible auroral powers. To detect our estimated Proxima b strength aurora ($\sim 10^{12}$ W), a coronagraph-equipped VLT would have to integrate for $\sim 1,000$ hours. However, if observations are scheduled during periods of vigorous stellar activity, during which the auroral output $\sim 10^{13}$ W (§2), an upgraded SPHERE may be able to detect the signal in about 10 hours. Note that for the VLT's 8.2m diameter, the SPHERE coronagraph must achieve an inner working angle no more than $\theta_{\rm IWA} = 2.7\lambda/D$ to extend as long as 5577Å given the maximal planet-star angular separation of 37 mas for Proxima b.

Future observations with a coronagraph-equipped TMT could observe our estimated Proxima b strength aurora in about 10 hours. If LUVOIR and HabEx launch with the capability to observe in a high-contrast, high-spectral resolution mode, LUVOIR could make the predicted observation in under 100 hours, while HabEx would require over 1000 hours.

4. SEARCH IN THE HARPS DATA

The Pale Red Dot (PRD) campaign (Anglada-Escudé et al. 2016) observed Proxima Centauri with HARPS for a total of 50 hours between 2005 and 2016. The spectra were taken in the wavelength range $3782 - 6913$Å with a resolving power $R = 115,000$, yielding a wavelength resolution $\Delta\lambda \approx 0.05$Å at 5577Å. Each wavelength bin was oversampled by a factor of about 5, for a total of $\sim$10 spectral elements across the FWHM of the OI line. Given the estimates in Table 3, if Proxima b's auroral power were on the order of 10^{15} W, the OI line could be detectable in that dataset. We therefore downloaded all 251 calibrated spectra from the ESO Archive[9] and searched them for the 5577Å feature.

We first shifted all spectra to the stellar rest frame by cross-correlating them against each other and calibrating the wavelength array to the stellar Na D I and II lines. Next, we removed stellar lines by performing weighted principal component analysis (WPCA; Delchambre 2015) on a 250Å window centered at 5577Å. Each spectrum was then fit with a linear combination of the first 25 principal components, a number which we obtained by optimizing the recovery efficiency of injected planetary signals (see below); the fit was then subtracted, reducing the noise in the vicinity of 5577Å by a factor of $\sim$7. In order to obtain the principal components, we weighted each spectrum by the square root of its exposure time and assigned weights of zero to the individual telluric 5577Å airglow features, as these are the among the strongest features in any individual spectrum and may incorrectly bias the principal components in the stellar frame; we remove Earth airglow separately below.

Next, we Doppler-shifted all spectra into the frame of Proxima b. Since the orbital inclination is unconstrained,

[9] http://archive.eso.org/

we performed this step multiple times, varying the inclination in one degree increments from 20° to 90°. We did not consider inclinations lower than 20° due to the difficulty of deconvolving stellar and planetary signals in near face-on orbits. Each iteration was itself performed fifty times, each time drawing the planet mass, planet period, stellar mass, and planet mean longitude from a normal distribution consistent with the values reported in Anglada-Escudé et al. (2016). For simplicity, the eccentricity was assumed to be zero, which is possible for certain assumptions for the initial orbital architecture of the Proxima Centauri planetary system (Barnes et al. 2016).

Once in the planet frame, we identified and linearly interpolated over $> 10\sigma$ outliers in each wavelength bin of the normalized spectra. We found that this successfully removed telluric airglow and prevented outlier features in individual spectra from contributing to the stacked spectrum, while still preserving coherent injected planetary features. We note that there is a potential pitfall in this process: if the planet's aurora is highly variable, differing by an order of magnitude or more across all the spectra, the signal may be removed during this step. We therefore performed a separate search in which we skipped this outlier removal step and instead removed telluric lines according to the method described in Brogi et al. (2012), in which individual wavelength bins are de-trended against a linear function of the airmass of each observation. In general, this latter method resulted in slightly noisier spectra and did not enhance the detectability of the planet signal, which as we argue below, is likely one or two orders of magnitude below our present detection limit.

Finally, for each orbital configuration, we co-added all spectra in the planet frame, omitting spectra in which the planetary 5577Å window overlapped with either the stellar or telluric 5577Å windows to avoid contamination from OI emission by those sources. For orbits close to edge-on, this reduced the total exposure time from 50 to about 40 hours, and less for lower inclination orbits. We then binned the stacked spectra to 0.1Å-wide bins and measured the strength of the planetary 5577Å signal as the number of standard deviations above the mean.

We find a peak at 5577Å for an orbital inclination of 69°, but this $\sim 2.3\sigma$ signal is entirely consistent with noise; see the left panel of Fig. 2. In order to use this non-detection to constrain the auroral power of Proxima b, we performed injection/recovery tests to assess the efficiency of our retrieval method. We injected Gaussian OI emission features with FWHM = 0.1Å and varying planet-star contrast into each of the raw spectra in the planet frame, and processed the spectra as explained above. Although we are able to detect the injected signal at $> 3\sigma$ down to a contrast ratio of 5×10^{-3}, we note that a much larger detection threshold is necessary for a robust detection, particularly given the fact that we stacked the spectra in 3,500 different ways to search for a signal. We therefore estimate our false alarm probability (FAP) as a function of the amplitude of the recovered signal by randomly shifting, stacking, and binning the processed spectra 5,000 times and computing a histogram of the deviations from the mean in each of the bins. We find that only one of $\sim 10^7$ bins had a signal $> 6\sigma$ from the mean. We therefore conservatively choose 8σ as the threshold for detection of OI emission from the planet, for which FAP $< 5 \times 10^{-8}$ (though likely lower than this value by a few orders of magnitude). In the HARPS dataset, this corresponds to a contrast ratio of 8×10^{-3} (right panel of the figure). Based on Table 3, this constrains the auroral power of Proxima b to be $\lesssim 4 \times 10^{15}$ W, consistent with the upper limits presented in §2.

We also performed similar searches for the red oxygen lines (6300 and 6364Å) and the 3914Å UV nitrogen line, which are prominent in Earth's aurora, but find no signal for any orbital configuration. Given the lower power in the red lines relative to the green line, and the low transmissivity of Earth's atmosphere and lower detector efficiencies in the UV, this non-detection is consistent with the non-detection of the 5577Å feature.

5. DISCUSSION AND CONCLUSIONS

Given the RV estimate of Proxima b's mass of $m\sin i \approx 1.27 M_\oplus$, the planet is likely terrestrial (Anglada-Escudé et al. 2016). However, due to the mass-inclination degeneracy, it is possible that Proxima b is more massive and on a close to face-on orbit, in which case it may be a mini-Neptune. In this case, its atmosphere may be dominated by H and He rather than by oxygen-bearing species. As we discussed in §2, a search for Lyman-Werner H_2 emission in the UV would be more appropriate in this case. Although broader than the lines we consider here, this emission is likely stronger (see §2), and is unlikely to be confused with stellar emission, given that it is molecular in origin. But perhaps more importantly, a robust *non*-detection of this and other H/He features could rule out a large gaseous envelope and confirm the terrestrial nature of the planet. That said, we are currently unable to efficiently probe near-face-on orbits due to the much smaller Doppler shift of the planetary lines. Observations made exclusively at quadrature, when the planet RV is highest, may help with this in the future.

In the more likely case that Proxima b is terrestrial, our HARPS search constrains its auroral power to be $< 4 \times 10^{15}$ W. This is consistent with the calculations in §2, which suggest the auroral power on Proxima b is likely on the order of 10^{12} W, or $\sim 100\times$ that of the Earth during steady-state solar wind conditions. Those calculations, however, ignore transient increases in stellar magnetic activity, which can enhance the auroral signal, and the diffuse airglow emission of the planet. As discussed in §2, transient magnetospheric activity could result in auroral power on the order of 10^{13} W. Future spectroscopic observations of Proxima Centauri may thus wish to observe during periods of vigorous magnetospheric activity.

Even if Proxima b is terrestrial, an auroral signal is not guaranteed to be present. The existence of an atmosphere is still an open question, owing to vigorous past hydrodynamic escape (Luger & Barnes 2015; Barnes et al. 2016), persistent stellar activity (Davenport et al. 2016) and an unconstrained planetary magnetic field. Even if an oxygen-rich atmosphere is present, nitrogen may need to be present to enhance the auroral signal. On Earth, ∼40% of the OI green line emission results from collisions with excited N_2^+ (Strickland et al. 2000). It is unclear whether or not other molecular species could

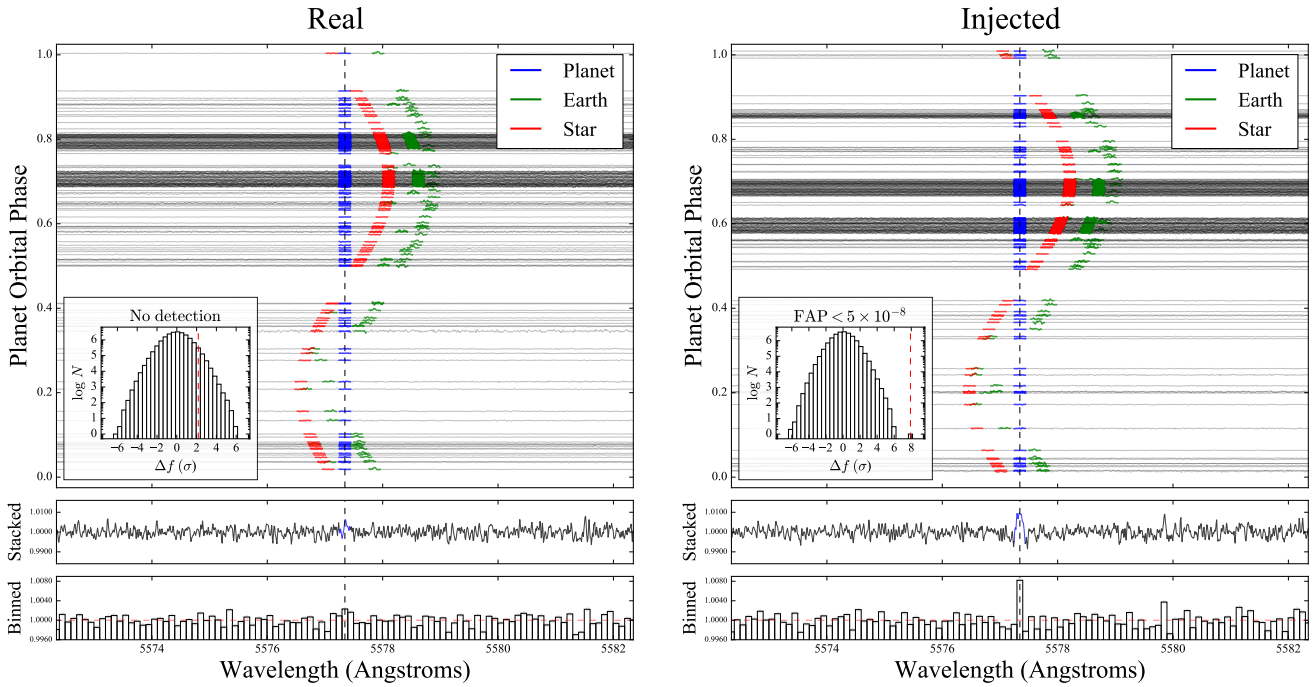

FIG. 2.— Analysis of the HARPS spectra of Proxima Centauri. After removing stellar and telluric lines, the individual spectra are Doppler-shifted into the frame of Proxima b and distributed vertically on the main subplots according to the planet's orbital phase. Blue regions indicate a 0.2Å window centered on the 5577Å oxygen feature in the planet frame. Red and green regions indicate the same window in the star and Earth frames, respectively; note the residual telluric airglow features in many of the spectra. The bottom subplots show the stacked spectrum in the planet frame and the stacked spectrum after downsampling to bins of size equal to the FWHM of the line. *Left column*: Our search results, assuming an orbital inclination of 69°, which yields the strongest signal. The inset at the bottom left shows a histogram of the amplitude of the deviations from the median computed over a 250Å window by randomly Doppler-shifting the spectra by small amounts and stacking them. The recovered signal is consistent with noise. *Right column*: Results for an emission feature injected into the raw data with contrast 8×10^{-3}. Our method recovers the signal in the stacked, binned spectrum at 8σ. From the histogram in the inset, we compute a false alarm probability (FAP) $\ll 5 \times 10^{-8}$. The non-detection in the left panel therefore constrains the auroral power on Proxima b to be $\lesssim 4 \times 10^{15}$ W, consistent with the calculations in §2.

play a similar role if N_2 is not the bulk atmospheric constituent. However, the detection of the 3914Å N_2^+ line could be a good diagnostic in the UV, where the star is even fainter. If we assume that the power of the 3914Å nitrogen line is comparable to that of the OI line (which is typical for higher energy magnetospheric particle populations), then the planet-star contrast in the N_2^+ line is an order of magnitude greater than at 5577Å. Since the strength of the N_2^+ line scales with magnetospheric parameters, stellar activity could cause strong transient features in the UV, which may be observable. Note, however, that limitations in UV detector efficiencies may complicate the detection of nitrogen and other UV aurorae.

A detection of an exo-aurora using the methods presented in §4 would place strong constraints on the eccentricity and break the $m\sin i$ degeneracy, leading to greater confidence in the terrestrial nature of Proxima b. Our non-detection places no such constraints, but our predicted telescope integration times of order 100 hours outline a path towards detecting auroral emission with reasonable upgrades to current and future facilities. We encourage further research into the use of high resolution spectroscopy with coronagraphic starlight suppression, particularly using low noise detectors that will allow substantial spectral downbinning with minimal added noise. Additionally, the development of effective optical AO and high contrast imaging systems is crucial for future observations aimed at optical auroral detection.

Our integration times using LUVOIR and HabEx suggest that they can be excellent observatories for the observation of aurora. However, such measurements would required a high resolution mode similar to the SPHERE and ESPRESSO coupling (Lovis et al. 2016). Furthermore, since read noise and dark current dominate the coronagraph noise budget, the development of low-noise detectors, e.g. MKIDS (Mazin et al. 2012, 2015), would significantly help the detection sensitivity and would allow such high-resolution spectroscopy to be downbinned to the lower resolution typically considered for direct exoplanet spectroscopy.

The methods of exo-auroral detection discussed here are not limited to Proxima b, but may be applicable to any exoplanet orbiting a nearby late-type star or brown dwarf. For example, the recently discovered TRAPPIST-1 system (Gillon et al. 2016) consists of three planets orbiting an active late M8 ultracool dwarf only 12 pc away; one planet in the system, TRAPPIST-1d, potentially lies in the habitable zone. Since TRAPPIST-1 is a later type star than Proxima Centauri, it is likely more active (e.g., West et al. 2008) and hence could generate larger particle fluxes and a stronger interplanetary magnetic field than Proxima Centauri, leading to more powerful aurorae on its planets. Additionally, TRAPPIST-1 is roughly 5× dimmer than Proxima Centauri at the OI 5577Å line, resulting in far more favorable contrast ratios. However,

due to its distance, auroral emission from this system will be $\sim 100\times$ dimmer than that from Proxima Centauri, likely making its detection infeasible. For coronagraphic observations, the distance to the TRAPPIST system would require an inner working angle smaller than the diffraction limit to extend as long as 5577Å for all known TRAPPIST-1 planets observed with a 10m class telescope, further complicating the observation.

Another planet to consider is GJ1132b, which orbits a M3.5 star 12 pc away (Berta-Thompson et al. 2015). Since it receives $\sim 19\times$ the Earth's flux and may have an O_2 rich atmosphere (Schaefer et al. 2016), it could display strong auroral emission. However, as with the TRAPPIST-1 system, its distance makes auroral characterization difficult. Moreover, the earlier type host emits a larger fraction of its light in the optical, resulting in a poorer auroral contrast ratio.

Finally, exoplanets orbiting nearby brown dwarfs may be prime targets for exo-auroral searches. Although no short-period exoplanets are currently known to orbit nearby brown dwarfs (He et al. 2016), the methods described in this paper may be used as means of exoplanet detection. Since the stack-and-search method described in §4 does not require previous RV observations of a system, a long baseline of spectroscopic observations of nearby M dwarfs and brown dwarfs could be used to search for Doppler-shifted 5577Å OI emission. Our method is particularly sensitive to short-period terrestrial planets, whose auroral power (if an atmosphere is present) is large and whose large RV will Doppler-shift the signal by one or more Å. Future high-resolution spectroscopy observations of our nearest neighbors could thus reveal the presence of unknown terrestrial exoplanets, including ones in the habitable zone.

6. ACKNOWLEDGEMENTS

We thank G. Anglada-Escude and the Pale Red Dot team for making their data publicly available. We thank Giada Arney for useful discussions. DPF is supported by an NSF IGERT DGE-1258485 fellowship. This work was supported by the NASA Astrobiology Institutes Virtual Planetary Laboratory under Cooperative Agreement number NNA13AA93A.

REFERENCES

Agol, E. 2007, MNRAS, 374, 1271
Anglada-Escudé, G., Amado, P. J., Barnes, J., Berdiñas, Z. M., Butler, R. P., Coleman, G. A. L., de La Cueva, I., Dreizler, S., Endl, M., Giesers, B., Jeffers, S. V., Jenkins, J. S., Jones, H. R. A., Kiraga, M., Kürster, M., López-González, M. J., Marvin, C. J., Morales, N., Morin, J., Nelson, R. P., Ortiz, J. L., Ofir, A., Paardekooper, S.-J., Reiners, A., Rodríguez, E., Rodríguez-López, C., Sarmiento, L. F., Strachan, J. P., Tsapras, Y., Tuomi, M., & Zechmeister, M. 2016, Nature, 536, 437
Barnes, R., Deitrick, R., Luger, R., Driscoll, P. E., Quinn, T. R., Fleming, D. P., Guyer, B., McDonald, D. V., Meadows, V. S., Arney, G., Crisp, D., Domagal-Goldman, S. D., Lincowski, A., Lustig-Yaeger, J., & Schwieterman, E. 2016, ArXiv e-prints
Bastian, T. S., Dulk, G. A., & Leblanc, Y. 2000, ApJ, 545, 1058
Berta-Thompson, Z. K., Irwin, J., Charbonneau, D., Newton, E. R., Dittmann, J. A., Astudillo-Defru, N., Bonfils, X., Gillon, M., Jehin, E., Stark, A. A., Stalder, B., Bouchy, F., Delfosse, X., Forveille, T., Lovis, C., Mayor, M., Neves, V., Pepe, F., Santos, N. C., Udry, S., & Wünsche, A. 2015, Nature, 527, 204
Beuzit, J.-L., Feldt, M., Dohlen, K., Mouillet, D., Puget, P., Wildi, F., Abe, L., Antichi, J., Baruffolo, A., Baudoz, P., Boccaletti, A., Carbillet, M., Charton, J., Claudi, R., Downing, M., Fabron, C., Feautrier, P., Fedrigo, E., Fusco, T., Gach, J.-L., Gratton, R., Henning, T., Hubin, N., Joos, F., Kasper, M., Langlois, M., Lenzen, R., Moutou, C., Pavlov, A., Petit, C., Pragt, J., Rabou, P., Rigal, F., Roelfsema, R., Rousset, G., Saisse, M., Schmid, H.-M., Stadler, E., Thalmann, C., Turatto, M., Udry, S., Vakili, F., & Waters, R. 2008, in Ground-based and Airborne Instrumentation for Astronomy II, ed. I. S. McLean & M. M. Casali (SPIE-Intl Soc Optical Eng)
Bhardwaj, A. & Gladstone, G. R. 2000, Reviews of Geophysics, 38, 295
Brogi, M., de Kok, R. J., Birkby, J. L., Schwarz, H., & Snellen, I. A. G. 2014, A&A, 565, A124
Brogi, M., Snellen, I. A. G., de Kok, R. J., Albrecht, S., Birkby, J., & de Mooij, E. J. W. 2012, Nature, 486, 502
Chamberlain, J. W. 1961, Physics of the aurora and airglow
Cheng, A. F. 1990, Geophysical Research Letters, 17, 1669
Cohen, O., Drake, J. J., Glocer, A., Garraffo, C., Poppenhaeger, K., Bell, J. M., Ridley, A. J., & Gombosi, T. I. 2014, ApJ, 790, 57
Connerney, J. E. P., Acua, M. H., & Ness, N. F. 1991, Journal of Geophysical Research: Space Physics, 96, 19023
Cowan, N. B., Agol, E., & Charbonneau, D. 2007, MNRAS, 379, 641
Crossfield, I. J. M., Hansen, B. M. S., Harrington, J., Cho, J. Y.-K., Deming, D., Menou, K., & Seager, S. 2010, ApJ, 723, 1436
Dalcanton, J., Seager, S., Aigrain, S., Battel, S., Brandt, N., Conroy, C., Feinberg, L., Gezari, S., Guyon, O., Harris, W., Hirata, C., Mather, J., Postman, M., Redding, D., Schiminovich, D., Stahl, H. P., & Tumlinson, J. 2015, ArXiv e-prints
Davenport, J. R. A., Kipping, D. M., Sasselov, D., Matthews, J. M., & Cameron, C. 2016, ArXiv e-prints
Delchambre, L. 2015, MNRAS, 446, 3545
Dempsey, J. T., Storey, J. W. V., & Phillips, A. 2005, PASA, 22, 91
Dou, J.-P., Ren, D.-Q., & Zhu, Y.-T. 2010, Research in Astronomy and Astrophysics, 10, 189
Driscoll, P. & Olson, P. 2011, Icarus, 213, 12
Faigler, S. & Mazeh, T. 2011, MNRAS, 415, 3921
Gillon, M., Jehin, E., Lederer, S. M., Delrez, L., de Wit, J., Burdanov, A., Van Grootel, V., Burgasser, A. J., Triaud, A. H. M. J., Opitom, C., Demory, B.-O., Sahu, D. K., Bardalez Gagliuffi, D., Magain, P., & Queloz, D. 2016, Nature, 533, 221
Gray, C. L., Chanover, N. J., Slanger, T. G., & Molaverdikhani, K. 2014, Icarus, 233, 342
Grießmeier, J.-M., Zarka, P., & Spreeuw, H. 2007, A&A, 475, 359
Guyon, O., Martinache, F., Cady, E. J., Belikov, R., Balasubramanian, K., Wilson, D., Clergeon, C. S., & Mateen, M. 2012, How ELTs will acquire the first spectra of rocky habitable planets
He, M. Y., Triaud, A. H. M. J., & Gillon, M. 2016, ArXiv e-prints
Hess, S. L. G. & Zarka, P. 2011, A&A, 531, A29
Hubert, B., Grard, J.-C., Evans, D. S., Meurant, M., Mende, S. B., Frey, H. U., & Immel, T. J. 2002, Journal of Geophysical Research: Space Physics, 107, SMP 15
Hunten, D. M., Rundle, H. N., Shepherd, G. G., & Vallance Jones, A. 1967, Appl. Opt., 6, 1609
Kivelson, M. G. & Russell, C. T. 1995, Introduction to Space Physics, 586
Knutson, H. A., Charbonneau, D., Allen, L. E., Burrows, A., & Megeath, S. T. 2008, ApJ, 673, 526
Knutson, H. A., Charbonneau, D., Allen, L. E., Fortney, J. J., Agol, E., Cowan, N. B., Showman, A. P., Cooper, C. S., & Megeath, S. T. 2007, Nature, 447, 183
Kouveliotou, C., Agol, E., Batalha, N., Bean, J., Bentz, M., Cornish, N., Dressler, A., Figueroa-Feliciano, E., Gaudi, S., Guyon, O., Hartmann, D., Kalirai, J., Niemack, M., Ozel, F., Reynolds, C., Roberge, A., Straughn, K. S. A., Weinberg, D., & Zmuidzinas, J. 2014, ArXiv e-prints

Kreidberg, L. & Loeb, A. 2016, ArXiv e-prints
Lovis, C., Snellen, I., Mouillet, D., Pepe, F., Wildi, F., Astudillo-Defru, N., Beuzit, J.-L., Bonfils, X., Cheetham, A., Conod, U., Delfosse, X., Ehrenreich, D., Figueira, P., Forveille, T., Martins, J. H. C., Quanz, S., Santos, N. C., Schmid, H.-M., Ségransan, D., & Udry, S. 2016, ArXiv e-prints
Luger, R. & Barnes, R. 2015, Astrobiology, 15, 119
Macintosh, B., Graham, J. R., Ingraham, P., Konopacky, Q., Marois, C., Perrin, M., Poyneer, L., Bauman, B., Barman, T., Burrows, A. S., Cardwell, A., Chilcote, J., Rosa, R. J. D., Dillon, D., Doyon, R., Dunn, J., Erikson, D., Fitzgerald, M. P., Gavel, D., Goodsell, S., Hartung, M., Hibon, P., Kalas, P., Larkin, J., Maire, J., Marchis, F., Marley, M. S., McBride, J., Millar-Blanchaer, M., Morzinski, K., Norton, A., Oppenheimer, B. R., Palmer, D., Patience, J., Pueyo, L., Rantakyro, F., Sadakuni, N., Saddlemyer, L., Savransky, D., Serio, A., Soummer, R., Sivaramakrishnan, A., Song, I., Thomas, S., Wallace, J. K., Wiktorowicz, S., & Wolff, S. 2014, Proceedings of the National Academy of Sciences, 111, 12661
Mauk, B. & Bagenal, F. 2012, Washington DC American Geophysical Union Geophysical Monograph Series, 197
Mauk, B. H., Krimigis, S. M., & Acua, M. H. 1994, Journal of Geophysical Research: Space Physics, 99, 14781
Maurin, A. S., Selsis, F., Hersant, F., & Belu, A. 2012, A&A, 538, A95
Mazin, B. A., Bumble, B., Meeker, S. R., O'Brien, K., McHugh, S., & Langman, E. 2012, Optics Express, 20, 1503
Mazin, B. A., Meeker, S., Strader, M., Szypryt, P., Walter, A., Bockstiegel, C., Collura, G., Mawet, D., Jensen-Clem, R., Guyon, O., Jovanovic, N., Oppenheimer, R., & Serabyn, E. 2015, in AAS/Division for Extreme Solar Systems Abstracts, Vol. 3, AAS/Division for Extreme Solar Systems Abstracts, 104.07
Meadows, V. S., Arney, G. N., Schwieterman, E. W., Lustig-Yaeger, J., Lincowski, A. P., Robinson, T., Domagal-Goldman, S. D., Barnes, R. K., Fleming, D. P., Deitrick, R., Luger, R., Driscoll, P. E., Quinn, T. R., & Crisp, D. 2016, ArXiv e-prints
Mennesson, B., Gaudi, S., Seager, S., Cahoy, K., Domagal-Goldman, S., Feinberg, L., Guyon, O., Kasdin, J., Marois, C., Mawet, D., Tamura, M., Mouillet, D., Prusti, T., Quirrenbach, A., Robinson, T., Rogers, L., Scowen, P., Somerville, R., Stapelfeldt, K., Stern, D., Still, M., Turnbull, M., Booth, J., Kiessling, A., Kuan, G., & Warfield, K. 2016, The Habitable Exoplanet (HabEx) Imaging Mission: preliminary science drivers and technical requirements
O'Malley-James, J. T. & Kaltenegger, L. 2016, ArXiv e-prints
Preusse, S., Kopp, A., Büchner, J., & Motschmann, U. 2007, Planetary and Space Science, 55, 589
Reiners, A. & Basri, G. 2008, A&A, 489, L45
Rimmer, P. B., Helling, C., Morley, C., Littlefair, S., & Hallinan, G. 2015, in AAS/Division for Extreme Solar Systems Abstracts, Vol. 3, AAS/Division for Extreme Solar Systems Abstracts, 104.15
Robinson, T. D., Stapelfeldt, K. R., & Marley, M. S. 2016, PASP, 128, 025003
Sandel, B. R., Herbert, F., Dessler, A. J., & Hill, T. W. 1990, Geophysical Research Letters, 17, 1693
Schaefer, L., Wordsworth, R., Berta-Thompson, Z., & Sasselov, D. 2016, ArXiv e-prints
Selsis, F., Wordsworth, R. D., & Forget, F. 2011, A&A, 532, A1
Service, R. W. 1907, The Cremation of Sam McGee in *Songs of a Sourdough* (Toronto: W. Briggs)
Seth, S., Haider, S., & Oyama, K. 2002, Journal of Geophysical Research: Space Physics, 107
Slanger, T. G., Cosby, P. C., Huestis, D. L., & Bida, T. A. 2001, Science, 291, 463
Smith, D. S., Scalo, J., & Wheeler, J. C. 2004, Icarus, 171, 229
Steele, D. P. & McEwen, D. J. 1990, Journal of Geophysical Research: Space Physics, 95, 10321
Stevenson, K. B., Désert, J.-M., Line, M. R., Bean, J. L., Fortney, J. J., Showman, A. P., Kataria, T., Kreidberg, L., McCullough, P. R., Henry, G. W., Charbonneau, D., Burrows, A., Seager, S., Madhusudhan, N., Williamson, M. H., & Homeier, D. 2014, Science, 346, 838
Strickland, D. J., Hecht, J. H., Christensen, A. B., & McEwen, D. J. 2000, Journal of Geophysical Research: Space Physics, 105, 2461
Turbet, M., Leconte, J., Selsis, F., Bolmont, E., Forget, F., Ribas, I., Raymond, S. N., & Anglada-Escudé, G. 2016, ArXiv e-prints
Vasyliunas, V. M., Kan, J. R., Siscoe, G. L., & Akasofu, S.-I. 1982, Planetary and Space Science, 30, 359
Wang, C., Han, J. P., Li, H., Peng, Z., & Richardson, J. D. 2014, Journal of Geophysical Research: Space Physics, 119, 6199
West, A. A., Hawley, S. L., Bochanski, J. J., Covey, K. R., Reid, I. N., Dhital, S., Hilton, E. J., & Masuda, M. 2008, AJ, 135, 785
Wood, B., Müller, H.-R., Zank, G., Izmodenov, V., & Linsky, J. 2004, Advances in Space Research, 34, 66
Wood, B. E., Müller, H.-R., Zank, G. P., Linsky, J. L., & Redfield, S. 2005, The Astrophysical Journal Letters, 628, L143
Zarka, P. 2007, Planet. Space Sci., 55, 598
Zellem, R. T., Lewis, N. K., Knutson, H. A., Griffith, C. A., Showman, A. P., Fortney, J. J., Cowan, N. B., Agol, E., Burrows, A., Charbonneau, D., Deming, D., Laughlin, G., & Langton, J. 2014, ApJ, 790, 53
Zuluaga, J. I. & Bustamante, S. 2016, ArXiv e-prints